Synthesis of silica-coated ferromagnetic fine powder by heterocoagulation

2008 J. Phys.: Condens. Matter 20 204105

(http://iopscience.iop.org/0953-8984/20/20/204105)

J. Phys.: Condens. Matter **20** (2008) 204105 (6pp) doi:10.1088/0953-8984/20/20/204105

Synthesis of silica-coated ferromagnetic fine powder by heterocoagulation

H S Park, G Dodbiba, L F Cao and T Fujita

Department of Geosystem Engineering, School of Engineering, The University of Tokyo, 7-3-1 Hongo, Bunkyo-ku, Tokyo 113-8656, Japan

E-mail: pppk22@empal.com (H S Park)

Received 31 March 2008
Published 1 May 2008
Online at stacks.iop.org/JPhysCM/20/204105

Abstract

In this paper, the synthesis of core–shell particles (i.e. temperature-sensitive ferrite (TSF) covered with silica) has been investigated. At first, TSF (mean diameter of 10 nm) was prepared by the coprecipitation method in an alkaline solution. Then, silica coating on the TSF surface was carried out by the controlled hydrolysis and condensation of tetraethyl orthosilicate (TEOS). The core–shell particles were formed by a surface precipitation procedure using TSF nanoparticles as a core material. The particles of silica were formed and these particles were then absorbed on the TSF nanoparticles. The coating procedure was described and explained by calculating the potential energies of interaction between the TSF and SiO_2 nanoparticles, according to the Derjarguin–Landau–Verwey–Overbeck (DLVO) theory. The coating process was found to be influenced by the pH and concentration of the TEOS precursor. The thickness of the silica layer on TSF cores was observed by means of transmission electron microscopy (TEM). The results showed that the optimum thickness of the SiO_2 layer on TSF core particles was obtained at pH 7.5, while the TEOS concentration was kept at 9 mM.

1. Introduction

Magnetic fluid (MF) is one of the intelligent fluids and is a suspension of nanosize ferrimagnetic or ferromagnetic particles in a carrier liquid [1]. MF exhibits some very interesting properties under applied magnetic field, among which is the change viscosity of the fluid under magnetic field [2, 3]. A promising application is the use of ferrofluids as liquid carriers in different heat-exchange devices as well as in devices for magnetocaloric energy conversion. Such systems may require ferrofluids with high thermomagnetic coefficients; however, the most widely used ferrofluids prepared by dispersing the magnetite nanoparticles cannot satisfy these requirements. Therefore, the development and synthesis of temperature sensitive magnetic nanoparticles for ferrofluids is of great interest [4]. Nowadays, composite particles consisting of a core coated with another compound have received considerable interest because of the promising technological applications of such materials. Coatings are applied to change the surface characteristics of a powder and consequently to improve, for instance, the dispersibility, the thermal stability, or the magnetic properties [5]. Moreover, in order to prevent iron particles from oxidation, a stable protective layer should be introduced on the surface [6]. Atarashi *et al* discussed the formation of a silica layer, which is generally known as a protective layer of iron, with precisely controlled thickness. Silica formed on the surface of magnetic nanoparticles can screen the magnetic dipolar attraction between magnetic nanoparticles. Different methods have been developed among which the sol–gel process has been frequently used for its advantages compared with other methods, i.e. low cost and surfactant-free [7]. Moreover, it has been reported that the value of specific magnetization decreases with increasing thickness of silica layer [8]. Within this frame, the aim of this work was to coat TSF with a silica layer (thickness less than 5 nm) and test the magnetic properties of the synthesized powder.

2. Theoretical background

Heterocoagulation is usually described by the Derjarguin–Landau–Verwey–Overbeck (DLVO) theory, which considers the interaction of London–van der Waals force and the electric double layer between particles in suspension. In this work, the results are explained within the frame of the DLVO theory.

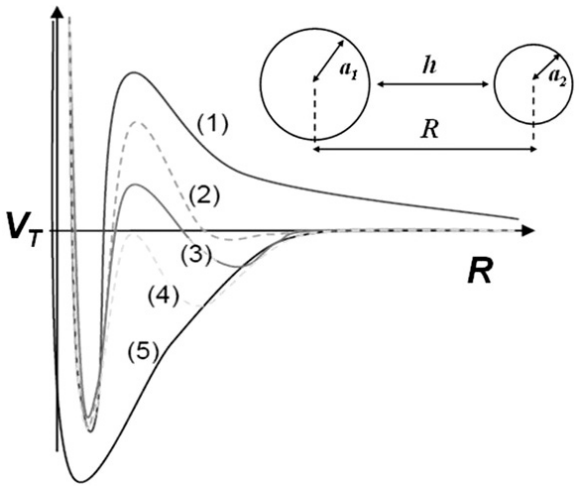

Figure 1. The interaction curve [12]. (1) Highly charged surfaces in dilute electrolyte, high energy barrier, stable colloid; (2) secondary minimum appears (typically >3 nm) energy barrier still too high, kinetically stable colloid; (3) lower energy barrier, slow coagulation; (4) energy barrier falls below ($V_T = R$), critical coagulation concentration, fast coagulation, unstable colloid; (5) no energy barrier, strong attraction, very fast coagulation.

The total interaction energy between colloid particles in an aqueous medium is given by equation (1), [9]:

$$V_T = V_A + V_R \tag{1}$$

where V_T is the total interaction energy, V_A is potential energy due to the London–van der Waals force, and V_R is the potential energy due to electrostatic interaction. Potential energy (V_A) due to the London–van der Waals force, acting between particles separated by a distance h is given by equation (2), [9]:

$$V_A = -\frac{A_{132}}{6}\left[\frac{2a_1a_2}{R^2-(a_1+a_2)^2} + \frac{2a_1a_2}{R^2-(a_1-a_2)^2} + \ln\left(\frac{R^2-(a_1+a_2)^2}{R^2-(a_1-a_2)^2}\right)\right] \tag{2}$$

where a_1 and a_2 are radii of particles, A is the Hamaker constant for the London–van der Waals force between particles, and R is defined as $R = a_1 + a_2 + h$ (figure 1). The Hamaker constant A_{132}, on the other hand, can be obtained by the following equation, (equation (3)) [9]:

$$A_{132} = \left(\sqrt{A_{11}} - \sqrt{A_{33}}\right)\left(\sqrt{A_{22}} - \sqrt{A_{33}}\right) \tag{3}$$

where A_{11} and A_{22} are the Hamaker constant of the particles and A_{33} is the Hamaker contents of the solution (in case that two particles are immersed in a solution). Moreover, the potential energy V_R of electrostatic interaction between spherical particles in solution is given by equation (4), [9]:

$$V_R = \frac{\pi\varepsilon_r\varepsilon_0 a_2(\psi_1^2+\psi_2^2)}{a_1+a_2}\left[\frac{2\psi_1\psi_2}{\psi_1^2+\psi_2^2}\ln\frac{1+\exp(-kh)}{1-\exp(-kh)} + \ln\{1-\exp(-2kh)\}\right] \tag{4}$$

where ψ_1, ψ_2 indicate the surface potential of the respective particles, whereas a_1 and a_2 are radii of the respective particles. κ is the Debye parameter, which is calculated by using [10]:

$$\kappa = \left(\frac{\sum z_i^2 n_i e^2}{\varepsilon_r\varepsilon_0 kT}\right)^{\frac{1}{2}} \tag{5}$$

where ε_0 is the electric constant of the solution, ε_r is the relative dielectric constant of the solution, n_i is the concentration of i^{-th} anion or cation in solution, e is the electron charge of the solution, z_i is the valence of the i^{-th} ion, k is the Boltzmann constant, and T is the absolute temperature.

Generally speaking, the interaction curve shows the amount of work, needed to bring one particle close to another. The potential barrier of the total potential energy (V_T) as a function of distance h between particles indicates the dispersion or the coagulation of a colloidal system [11]. The interaction curve is illustrated in figure 1. It should be noted that the interaction curves may look different from the typical curve due to fact that the interparticle interaction depends on the surface charge, electrolyte concentration, particle size and shape, the Hamaker constant, etc (equations (1)–(5)) [12].

3. Experimental details

3.1. Materials

The following materials were used for the synthesis of the TSF nanoparticles: iron (III) chloride hexahydrate ($FeCl_3{\cdot}6H_2O$, Nacalai, 99%), zinc chloride ($ZnCl_2$, Nacalai, 98%), nickel (II) chloride hexahydrate ($NiCl_2{\cdot}6H_2O$, Nacalai, 98%), calcium chloride dehydrate ($CaCl_2{\cdot}2H_2O$, Nacalai, 99%), sodium hydroxide (NaOH, Nacalai, 96%) and distilled water. For the preparation of silica-coated TSF nanoparticles, on the other hand, ethanol (C_2H_5OH, Nacalai, 99.5%), tetraethyl orthosilicate (TEOS, 95%, Wako), ammonia solution (NH_4OH, Wako, 28%) and 1 mol l^{-1} acetic acid (CH_3COOH, Nacalai) were also used. In addition, ammonium acetate (CH_3COONH_4, Nacalai, 97%) was added in the reaction solution as catalysis for the nucleation of SiO_2 particles.

3.2. Synthesis of temperature sensitive ferrite

Calcium-included Ni–Zn ferrite nanoparticles were prepared using the chemical coprecipitation method. Details of the preparation of TSF nanoparticles have been given in a previous publication [13]. A mixed aqueous solution of $NiCl_2{\cdot}6H_2O$, $CaCl_2{\cdot}2H_2O$, $ZnCl_2$ and $FeCl_3{\cdot}6H_2O$ in their respective stoichiometry at $Ni_{0.3}Ca_{0.1}Zn_{0.6}Fe_2O_4$, (i.e. the initial composition for coprecipitation Ni:Ca:Zn:Fe = 0.3:0.1:0.6:2 mol) was precipitated using 6M NaOH solution. The Fe, Ni, Ca, and Zn salts were dissolved separately in water and then 6M NaOH was added into the mixture solution until pH 12.5 was reached. This mixture was reacted at 368 K under constant mechanical stirring for 3600 s. The resulting TSF nanoparticles were then collected and separated from the reaction medium by using a permanent magnet. The synthesized particles was then washed several times with distilled water, followed by magnetic decantation. Finally, TSF nanoparticles were re-dispersed in distilled water.

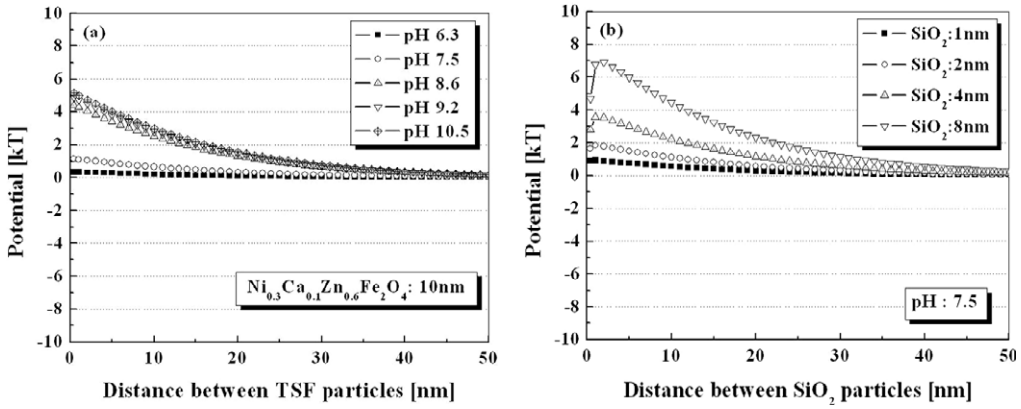

Figure 2. The interaction curves (a) interaction energy between TSF particles at various pH conditions, (b) interaction energy between SiO_2 particles at pH 7.5.

Table 1. Parameters used for the calculation of interaction energy [15–17].

	Water	TSF	SiO_2
A (Hamaker constant, $\times 10^{-20}$ J) [16, 17]	4.38	4	0.3
a (radius of particles, nm)	—	5	1–4
ψ (zeta potential, mV) [15]	—	10.0 (pH 6.3)	−48.0 (pH 6.3)
	—	−18.0 (pH 7.5)	−55.0 (pH 7.5)
	—	−35.0 (pH 8.6)	−58.0 (pH 8.5)
	—	−37.0 (pH 9.2)	−60.0 (pH 9.2)
	—	−38.0 (pH 10.5)	−57.0 (pH 10.5)

ε_0 (vacuum): 8.85×10^{-12}, ε_r (H_2O, at 323 K): 69.88, T (reaction temperature): 323 K

3.3. Preparation of silica-coated TSF nanoparticles

Coating TSF nanoparticles with silica was carried out in an alcohol/water (4:1 v/v%) mixture, containing TSF particles as core materials. The 0.5 M of CH_3COONH_4 was also added as a catalyst in the sample. Then, under continuous mechanical stirring, TEOS was added. After stirring for 3600 s, silica was formed and absorbed on the surface of TSF nanoparticles due to the hydrolysis and the condensation of TEOS. Before adding TEOS, the pH was adjusted in the range between 6.3 and 10.5 by adding CH_3COOH or NH_4OH. The suspension was stirred using a Teflon-coated propeller, while the temperature was kept constant at 323 K. The synthesized particles were then washed several times with ethanol. The particles, collected by means of filtration, were then dried in a desiccator at room temperature for two days.

3.4. Measurements

The morphology of core–shell type nanoparticles and the thickness of silica layer were observed by using a transmission electron microscope (JEM-2000EXII, JAPAN). A vibrating sample magnetometer (VSM) was also employed to investigate the magnetic properties of the prepared samples. The applied magnetic field was varied from 0.039 to 0.973 T. The measurements of magnetic properties were carried out at room temperature, using a sphere made of Ni as a reference material.

4. Results and discussion

4.1. Interaction energy between nanoparticles

Generally speaking, the interparticle interaction depends not only on the particle distance, but also on the surface charge and the particle size (figure 1). Both the surface charge of core particles and coating layers can be influenced by varying the pH values. The effect of pH and particle size on the behavior of the aggregation or dispersion of colloidal particles can be explained within the frame of DLVO theory. It should be noted that the dipolar interaction is negligible, since the magnetic susceptibility of silica particles is very small. Therefore, the magnetic field intensity almost did not affect the potential energy of interaction between magnetic particles and silica particles [14]. Parameters used for the calculation of interaction energy are tabulated in table 1 and the calculation results are shown in figure 2. The values of zeta potentials inputted in equation (4) are from a previous paper [15].

Figure 2 shows the interaction curves calculated by using equations (1)–(5). The interaction energy curve for TSF–TSF particles at pH values of 6.3, 7.5, 8.6, 9.2, and 10.5 are given in figure 2(a). It should be noted that the heights of the interaction energy barrier (figure 2(a)) are only for comparison. At pH 6.3, the TSF particles aggregate because the potential barrier is low due to a low zeta potential (10 mV, table 1). Similar behavior can be predicted at pH 7.5, but colloidal stability is a little higher than in the case of pH 6.3. On the other hand, TSF particles cannot be coagulated above pH 8.6 due to the presence of a relatively large positive potential

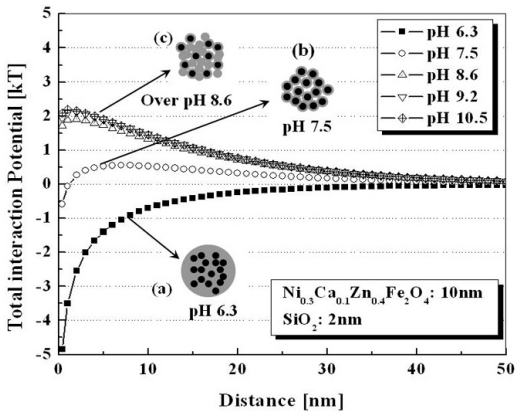

Figure 3. The interaction energy curve between TSF–SiO_2 particles at various pH conditions: (a) 6.3, (b) 7.5, and (c) 8.6, 9.2, and 10.5.

barrier and a high value of zeta potential ($\geqslant$35 mV, table 1), especially when compared with other cases (figure 2(a)). The total interaction energy for SiO_2–SiO_2 dispersed in a medium at pH 7.5 was calculated as a function of particle size and is shown in figure 2(b). It can be seen that, with the increase of the particle size, the height of the interaction energy barrier increases, indicating an increase of the dispersive stability of the SiO_2 suspension (figure 2(b)).

4.2. Coating of TSF nanoparticles with a silica layer

4.2.1. Effect of pH. Depending on the experimental conditions, three scenarios may arise, while the distinction may not always be clear. First, a dispersion of independent SiO_2 nanocrystals may form. When this occurs, a mixed system is obtained where the seed particles (TSF nanoparticles) and the newly precipitated phase (SiO_2) coexist as separate phases [18]. The second scenario is that the crystalline SiO_2 particles may independently precipitate and interact to various degrees with the TSF nanoparticles, forming a coating around the TSF nanoparticles [19]. Lastly, the reactants may adsorb onto the surface of the seed particles and the SiO_2 crystals may directly precipitate on the seed particles through surface nucleation and growth [20].

The pH influences both the precipitation rate of silicon dioxide and the surface charge of the two species that undergo heterocoagulation. The interaction curves between TSF-SiO_2 particles in the pH value between 6.3 and 10.5 are shown in figure 3, indicating the possible structure of the aggregation. At pH 6.3, TSF nanoparticles were aggregated due to a low potential barrier, since the surface of TSF is positively charged, whereas the surface of SiO_2 is negatively charged (figure 3(a), table 1). Due to the electrostatic attraction between them, small SiO_2 nanoparticles can be adsorbed onto the surface of aggregated TSF particles. At pH 7.5 (figure 3(b)), both TSF and formed SiO_2 particles are negatively charged, resulting in an electrostatic repulsion between these two particles. However, the total interaction energy between TSF-SiO_2 is relatively low. Hence, coating by heterocoagulation will occur (figure 3(b)). Above pH 8.6 (figure 3(c)), coating due to the heterocoagulation is expected, but the formation of some SiO_2 particles is also predicted because, in this case, NH_4OH was added in order to control the pH at a value higher than 8. In the sol–gel process, the presence of ammonia promotes the formation of SiO_2 spherical particles [21, 22].

In addition, a look at the TEM micrographs of silica-coated TSF particles at various pH conditions shows that at pH 6.3 (figure 4(a)), the surface coverage of SiO_2 on core particles was thicker than when the pH was kept at 7.5, since the TSF nanoparticles have a positive charge, whereas the precipitated SiO_2 particles have a negative charge (table 1). The optimum thickness of silica layer on core particles was achieved at pH 7.5 (figure 4(b)). Above pH 8.6 (figure 4(c)), an SiO_2 layer on the core particles was observed but some SiO_2 particles coagulated due to the promotion of SiO_2 particles by using ammonia as catalyst.

4.2.2. Effect of TEOS concentration. In order to gain some insight into the final thickness of silica layer, a set of calculations has been carried out. The hypotheses were as follows: particles are spherical and monodisperse (10 nm in diameter), and each particle is covered with silica. Then, a set of experiments was carried out at several concentrations of TEOS. The conditions for silica-coated TSF nanoparticles are listed in table 2. To study the influence of TEOS concentration on the silica-coated TSF nanoparticles, experiments were conducted at TEOS concentrations of 9, 25, and 86 mM, respectively. The concentration of TEOS was calculated to adjust the thickness of the silica layer to 2, 4, or 8 nm respectively.

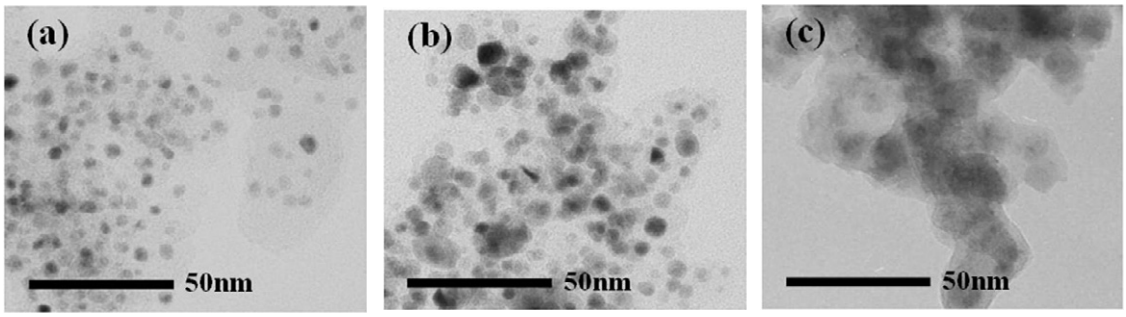

Figure 4. TEM micrographs of silica-coated TSF particles at various pH conditions: (a) 6.3, (b) 7.5, and (c) 8.6.

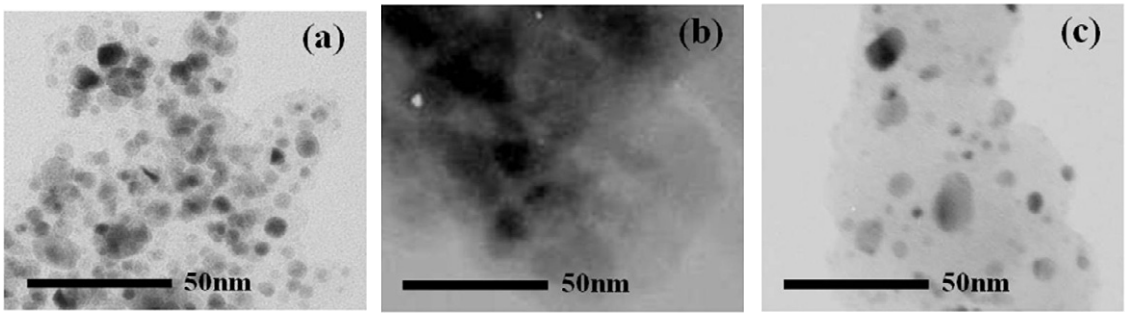

Figure 5. TEM micrographs of silica-coated TSF particles as a function of TEOS concentration: (a) 9 mM, (b) 25 mM, and (c) 86 mM.

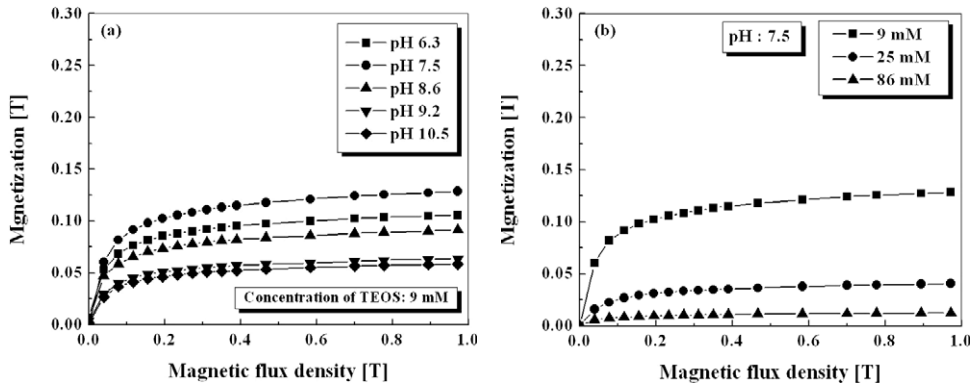

Figure 6. Magnetization curve: (a) silica-coated TSF nanoparticles as a function of pH; (b) silica-coated TSF nanoparticles as a function of TEOS concentration.

Table 2. The conditions for silica-coated TSF nanoparticles.

pH	Concentration of TEOS (mM)	The calculated silica layer (nm)
6.3, 7.5, 8.6, 9.2, 10.5	9	2
7.5	25	4
7.5	86	8

The TEM micrographs are shown in figure 5. It can be seen that at 9 mM a silica layer with a thickness of about 5 nm was observed (figure 5(a)). Further increase in concentration resulted in a thicker coating layer (figures 5(b) and (c)). Nevertheless, the thickness of silica layer is thicker than the calculated thickness of the layer. The reason for this difference may be due to the polydispersity of TSF particles and their shape, which was considered to be spherical.

4.3. Saturation magnetization of silica-coated TSF nanoparticles

In order to observe the saturation magnetization of silica-coated TSF nanoparticles, the magnetization as a function of magnetic flux density was measured by means of a VSM. The values of magnetization were measured in emu g^{-1} and then converted to tesla, after the density of the core–shell type particle was estimated, considering the volume and the mass of each coated particle as well as the average thickness of the silica layer observed from TEM.

Figure 6 shows the magnetization curve of as-synthesized powder samples at room temperature. The magnetization curves of the powders obtained at different pH values are shown in figure 6(a), whereas those obtained at different concentrations of TEOS are shown in figure 6(b). It can be seen that the saturation magnetization of silica-coated TSF nanoparticles synthesized at pH 7.5 was larger than the other samples (figure 6(a)). These experimental results pointed out that the saturation magnetization of silica-coated TSF nanoparticles is affected not only by the aggregation structure but also by the thickness of the silica layer.

5. Conclusions

In this study, the coating of TSF nanoparticles with a silica layer was investigated. The results showed that the aggregation structure and the thickness of the silica layer strongly depend on the experimental conditions such as the pH of the aqueous solution and the concentration of the TEOS precursor. The optimum thickness of the SiO_2 layer (thickness about 5 nm) on core particles was obtained at pH 7.5, while the TEOS concentration was kept at 9 mM. The experimental results showed that the saturation magnetization of silica-coated TSF nanoparticles decreased as the TEOS concentration increased, due to the existence of a non-magnetic silica layer. It has also been demonstrated that various thicknesses of coating layer and aggregation structure can be obtained by controlling the colloidal stability and the experimental conditions (pH and TEOS concentration).

Acknowledgments

This research was supported by the 21st Century COE Program, [Mechanical Systems Innovation] and the JSPS Postdoctoral Fellowship for Foreign Researches (FY2006).

References

[1] Kinnari P 2000 *Bull. Mater. Sci.* **23** 91
[2] Rosensweing R E 1969 *J. Colloid Interface Sci.* **20** 680
[3] Odenbach S 2004 *J. Phys.: Condens. Matter* **16** 1135
[4] Auzans E 1999 *Thesis* Institute of Physics, Latvian University
[5] Geuzens E *et al* 2006 *J. Eur. Ceram. Soc.* **26** 3133
[6] Atarashi T, Kim Y S, Fujita T and Nakatsuka K 1999 *J. Magn. Magn. Mater.* **201** 7
[7] Deng Y H, Wang C C, Hu J H, Yang W L and Fu S K 2005 *Colloids Surf.* A **262** 87
[8] Fu W, Yang H, Bala H, Liu S, Li M and Zou G 2006 *Mater. Lett.* **60** 1728
[9] Usui S 1989 *J. Assoc. Mater. Eng. Res.* **2** 171
[10] Elimelech M, Gregory J, Jia X and William R A 1995 *Particle Deposition and Aggregation: Measurement, Modeling, and Simulation* (Oxford: Butterworth-Heinemann) p 13
[11] Kitahara A and Watanabe A 1972 *Electrical Phenomena at Interfaces* (Tokyo: Kyoritsu) p 54
[12] Israelachvili J 1992 *Intermolecular and Surface Forces* (New York: Academic)
[13] Fujita T, Mamiya M and Jeyadevan B 1990 *J. Soc. Mater. Eng. Res.* **1** 43
[14] Garcia-Martinez H A *et al* 2005 *J. Dispers. Sci. Technol.* **26** 177
[15] Fujita T and Mamiya M 1989 *J. Japan Soc. Powder Powder Metall.* **36** 778 (in Japanese)
[16] Gherardi P and Matijevic E 1986 *J. Colloid Interface Sci.* **109** 57
[17] Wang G and Nicholson P S 2001 *J. Am. Ceram. Soc* **84** 1250
[18] Hiemenz P C and Rajagopalan R 1997 *Principles of Colloid and Surface Chem.* 3rd edn (New York: Dekker) p 485
[19] Kawahashi N and Matijevic E 1990 *J. Colloid Interface Sci.* **138** 534
[20] Philipse A P, van Bruggen M and Pathmamanoharan C 1994 *Langmuir* **10** 92
[21] Hench L L and West J K 1990 *Chem. Rev.* **90** 33
[22] Beydoun D 2000 *Thesis* The University of New South Wales